

Orthogonality catastrophe and Kondo effect in graphene.

Martina Hentschel

Max Planck Institut für Physik komplexer Systeme. Nöthnitzer Str. 38. D-01187 Dresden. Germany.

Francisco Guinea

Instituto de Ciencia de Materiales de Madrid. CSIC. Sor Juana Inés de la Cruz 3. E-28049 Madrid. Spain.

Anderson's orthogonality catastrophe in graphene, at energies close to the Dirac point, is analyzed. It is shown that, in clean systems, the orthogonality catastrophe is suppressed, due to the vanishing density of states at the Dirac point. In the presence of preexisting localized states at the Dirac energy, the orthogonality catastrophe shows similar features to those found in normal metals with a finite density of states at the Fermi level. The implications for the Kondo effect induced by magnetic impurities, and for the Fermi edge singularities in tunneling processes are also discussed.

PACS numbers: 73.20.-r; 73.20.Hb; 73.23.-b; 73.43.-f, 72.15.Qm

INTRODUCTION.

Graphene has attracted a great deal of attention recently, due to its novel fundamental properties and potential applications[1, 2, 3, 4, 5]. It is by now well established that its electronic properties at low energies are well described by the two dimensional Dirac equation. At half filling graphene should be a semimetal, with a vanishing density of states. This fact implies that many properties of a metal, which are parametrized by the density of states at the Fermi level, are different in a clean graphene sample. The description of the electronic bands in graphene based on the Dirac equation also leads to localized states in samples with edges[6, 7] or lattice defects[8, 9]. These states change the density of states near the Dirac energy, as they induce a peak at this energy. Hence, the density of states of graphene at the Dirac energy can either vanish, in a clean sample, or diverge, if localized states are induced.,

We study here Anderson's orthogonality catastrophe (AOC)[10] in clean and dirty graphene. The AOC can be considered the simplest non trivial feature in the response of a metal, and it is dependent on the value of the density of states at the Fermi level. The AOC directly leads to many singularities in experiments which probe the dynamical response of a metal, like the Fermi edge singularity in X-ray absorption[11, 12], and singularities in the transport properties of quantum dots and metallic grains[13, 14, 15]. In graphene, the interplay between the AOC and Coulomb blockade may be relevant for the analysis of transport experiments on small quantum dots[5, 16].

The Kondo effect induced by magnetic impurities in metals can be seen as a direct consequence of Anderson's orthogonality catastrophe[17, 18]. The coupling between the impurity spin and the conduction electrons can be divided into a transverse term, J_{\perp} , which leads to spin-flip processes, and a longitudinal term, J_{\parallel} , which induces an AOC associated to the same spin flips. This AOC leads

to a strong suppression of spin fluctuations, although the effects of J_{\perp} prevail at the lowest temperatures. These two competing processes can be defined, in a very transparent way, in the dissipative two level system[19], which is equivalent to the Kondo Hamiltonian. The Kondo temperature, T_K , can be seen as the scale at which spin flip processes ultimately cut off the AOC.

The AOC is modified in disordered metals[20] and ballistic mesoscopic systems, due to the changes in the electronic wavefunctions[21, 22]. We will analyze the AOC in graphene using the numerical methods explained in[21, 22] (see also[23]), and also a phaseshift analysis similar to that in[10].

We analyze first the phaseshifts induced by a local potential, first in clean graphene, and then in graphene in the presence of preexisting localized levels. The next section presents a numerical study of the full overlap between the electronic ground state before and after the potential is turned on, and an analysis of the scaling of this quantity with system size. The last section discusses the main implications of our work for the Kondo effect in graphene, and the Fermi edge singularities associated to tunneling processes.

PHASESHIFT ANALYSIS.

The overlap S between the Slater determinants which describe the electronic wavefunction before and after a potential is switched on can be written as[10]:

$$S \leq N \sum_l \frac{2l+1}{3\pi^2} \sin^2(\delta_l) \quad (1)$$

where N is the number of electrons, and δ_l is the phase-shift induced by the potential in the scattered waves at the Fermi level with angular momentum l . In a typical metal, a weak local potential of strength $\epsilon_0 \ll \epsilon_F$ induces a phaseshift in the s channel which can be approximated by $\delta_0 \approx \epsilon_0 N(\epsilon_F) \ll 1$, where $N(\epsilon_F)$ is the density of states at the Fermi level.

This analysis can be extended in a straightforward way to graphene, where the electronic wavefunctions can be approximated by the two dimensional Dirac equation (see below):

$$\mathcal{H} \equiv v_F \begin{pmatrix} 0 & \pm k_x + ik_y \\ \mp k_x + ik_y & 0 \end{pmatrix} \quad (2)$$

where the two signs correspond to the two inequivalent corners of the Brillouin Zone of the honeycomb lattice.

We use eq.(1) in order to describe the dependence of the overlap on the number of electrons, by computing analytically the phaseshifts induced by different types of potentials. In the following, we use energy and momentum units such that $v_F = 1$.

Clean graphene.

We analyze first the phaseshifts induced by a circular potential well in clean graphene, and we describe the electronic wavefunctions using the continuum Dirac equation, eq.(2). We expect that this approximation will describe qualitatively the effects of a local perturbation in the graphene lattice.

We assume that the potential well can scatter electrons between the K and K' valleys, as it is the case for sufficiently localized potentials in graphene.

Using cylindrical coordinates, the Hamiltonian in the clean system can be written as:

$$\mathcal{H} \equiv \begin{pmatrix} 0 & ie^{-i\phi}\partial_r + \frac{e^{-i\phi}}{r}\partial_\phi & 0 & 0 \\ ie^{i\phi}\partial_r - \frac{e^{-i\phi}}{r}\partial_\phi & 0 & 0 & 0 \\ 0 & 0 & 0 & -ie^{i\phi}\partial_r + \frac{e^{i\phi}}{r}\partial_\phi \\ 0 & 0 & -ie^{-i\phi}\partial_r - \frac{e^{-i\phi}}{r}\partial_\phi & 0 \end{pmatrix} \quad (3)$$

where the two first entries correspond to the K point, and the two last ones to the K' point.

We add a constant perturbation in the region $r \leq R_0$:

$$V \equiv \begin{pmatrix} \epsilon_0 & 0 & 0 & \Delta \\ 0 & \epsilon_0 & \Delta & 0 \\ 0 & \Delta & \epsilon_0 & 0 \\ \Delta & 0 & 0 & \epsilon_0 \end{pmatrix} \quad (4)$$

where ϵ_0 is a constant energy shift, and Δ is a potential which induces scattering between the two valleys, and it is compatible with the symmetries of the honeycomb lattice[24].

We analyze the scattering of an incident s wave with incoming energy k :

$$\Psi_{\text{inc}}(r, \phi) \equiv \begin{pmatrix} J_0(kr) \\ -iJ_1(kr)e^{i\phi} \\ 0 \\ 0 \end{pmatrix} \quad (5)$$

where $J_0(x)$ and $J_1(x)$ are Bessel functions of the

first kind. They satisfy: $\lim_{x \rightarrow 0} J_0(x) \approx 1$, and $\lim_{x \rightarrow 0} J_1(x) \approx x/2$.

The reflected waves outside the well can be written as:

$$\Psi_{\text{ref}}(r, \phi) \equiv R_1 \begin{pmatrix} Y_0(kr) \\ -iY_1(kr)e^{i\phi} \\ 0 \\ 0 \end{pmatrix} + R_2 \begin{pmatrix} 0 \\ 0 \\ iY_1(kr)e^{i\phi} \\ Y_0(kr) \end{pmatrix} \quad (6)$$

$Y_0(x)$ and $Y_1(x)$ are Bessel functions of the second kind. They satisfy: $\lim_{x \rightarrow 0} Y_0(x) \approx 2/\pi(\log(x/2) + \gamma)$, and $\lim_{x \rightarrow 0} Y_1(x) \approx -2/(\pi x)$. The first contribution on the right hand side of eq.(6) is a reflected wave in the same valley, and the second term is a wave in the opposite valley as the incident wave.

Inside the potential well, the spectrum has a gap for energies $\epsilon_0 - \Delta \leq \epsilon \leq \epsilon_0 + \Delta$. Within this range of energies, the wavefunction inside the well can be written as:

$$\Psi_{\text{trans}}(r, \phi) \equiv T_1 \begin{pmatrix} \frac{\sqrt{\Delta^2 - k'^2}}{\sqrt{2}\Delta} I_0(k'r) \\ +i\frac{k'}{\sqrt{2}\Delta} I_1(k'r)e^{i\phi} \\ 0 \\ \frac{1}{\sqrt{2}} I_0(k'r) \end{pmatrix} + T_2 \begin{pmatrix} \frac{ik'}{\sqrt{2}\Delta} I_0(k'r) \\ \frac{\sqrt{\Delta^2 - k'^2}}{\sqrt{2}\Delta} I_1(k'r)e^{i\phi} \\ i\frac{1}{\sqrt{2}} I_1(k'r)e^{i\phi} \\ 0 \end{pmatrix} \quad (7)$$

$I_0(x)$ and $I_1(x)$ are modified Bessel functions of the first kind. They satisfy: $\lim_{x \rightarrow 0} I_0(x) \approx 1$, and $\lim_{x \rightarrow 0} I_1(x) \approx x/2$. The value of k' in eq.(7) is given by: $\epsilon = \sqrt{\Delta^2 - k'^2}$. As $k = \epsilon + \epsilon_0$, we have $k' = \sqrt{\Delta^2 - (k - \epsilon_0)^2}$.

For $|\epsilon - \epsilon_0| \geq \Delta$, we have:

$$\Psi_{\text{trans}}(r, \phi) \equiv T_1 \begin{pmatrix} \frac{1}{\sqrt{2}\Delta} J_0(k'r) \\ -i \frac{\Delta}{\sqrt{2(\Delta^2 + k'^2)}} J_1(k'r) e^{i\phi} \\ 0 \\ \frac{\Delta}{\sqrt{2(\Delta^2 + k'^2)}} J_0(k'r) \end{pmatrix} + T_2 \begin{pmatrix} \frac{i\Delta}{\sqrt{2(\Delta^2 + k'^2)}} J_0(k'r) \\ \frac{1}{\sqrt{2}\Delta} J_1(k'r) e^{i\phi} \\ \frac{\Delta}{\sqrt{2(\Delta^2 + k'^2)}} J_1(k'r) e^{i\phi} \\ 0 \end{pmatrix} \quad (8)$$

and $\epsilon = \sqrt{\Delta^2 + k'^2}$, and $k' = \sqrt{(k - \epsilon_0)^2 - \Delta^2}$.

The scattering phaseshifts are determined by the reflection coefficients R_1 and R_2 defined in eq.(6). The boundary conditions at $r = R_0$ are simply the continuity of the spinors, which define a set of four equations for the four variables R_1, R_2, T_1 and T_2 .

For $\Delta = 0$ we have $R_2 = T_2 = 0$ and $R_1 = \bar{R}$. As $\lim_{x \rightarrow \infty} J_0(x) \approx \sqrt{2/(\pi x)} \cos(x - \pi/4)$, and $\lim_{x \rightarrow \infty} Y_0(x) \approx \sqrt{2/(\pi x)} \sin(x - \pi/4)$, the phaseshift δ is $\tan(\delta) = \bar{R}$. We find:

$$\tan(\delta) = \bar{R}(kR_0) = -\frac{J_1[(k - \epsilon_0)R_0]J_0(kR_0) - J_0[(k - \epsilon_0)R_0]J_1(kR_0)}{J_1[(k - \epsilon_0)R_0]Y_0(kR_0) - J_0[(k - \epsilon_0)R_0]Y_1(kR_0)} \quad (9)$$

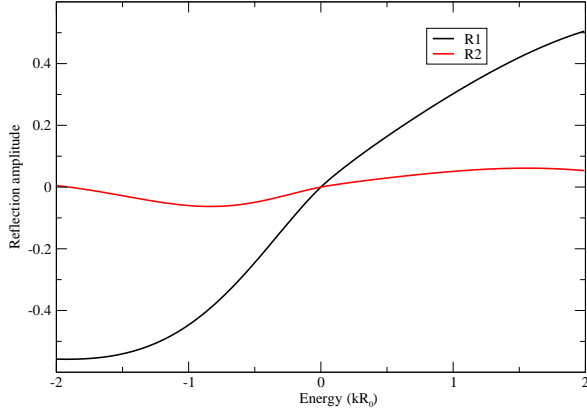


FIG. 1: (Color online). Reflection coefficients of a circular well with $\epsilon_0 R_0 = 0.5$ and $\Delta R_0 = 0.1$.

and:

$$\lim_{kR_0 \rightarrow \infty} \bar{R}(kR_0) = \tan(\epsilon_0 R_0) \quad (10)$$

Results for $\epsilon_0 R_0 = 0.5$ and $\Delta R_0 = 0.1$ are shown in Fig.[1]. In all cases, with or without (eq.(9)) intervalley scattering, the reflection coefficients vanish at the Dirac point, $k = 0$. This result can be simply understood by noting that a finite reflection coefficient implies a reflected wavefunction with a component $Y_1(kr)$ which diverges as $k \rightarrow 0$. The phaseshift vanishes linearly as $k \rightarrow 0$, in agreement with general arguments based on the vanishing of the density of states at the Dirac point.

The vanishing of the phaseshift at the Dirac point implies that the overlap between the Slater determinants before and after the potential is switched on does not scale like some power of the number electrons, and the AOC does not take place at this energy.

Phaseshift analysis in the presence of a localized state.

We will neglect here possible intervalley scattering terms. We study the phaseshifts induced by a weak potential near the edges of a circular void which supports surface states. A sketch of the model is shown in Fig.[2]. We write the wavefunction as:

$$\Psi(\tilde{\mathbf{r}}) \equiv \begin{pmatrix} \psi_1(\tilde{\mathbf{r}}) \\ \psi_2(\tilde{\mathbf{r}}) \end{pmatrix} \quad (11)$$

The edge of a crack, or extended vacancy is modeled by the boundary condition:

$$\psi_1(\tilde{\mathbf{r}}) = 0, \quad \tilde{\mathbf{r}} \in \Omega \quad (12)$$

where Ω is the boundary of the void.

We analyze a circular void, of radius R' . The boundary condition, eq.(12), allows for solutions at zero energy of the type:

$$\Psi(\tilde{\mathbf{r}}) \equiv \begin{pmatrix} 0 \\ \frac{e^{\pm i n \theta}}{r^n} \end{pmatrix} \quad (13)$$

where the two signs correspond to the two inequivalent corners of the Brillouin zone.

Eq.(12) implies, for s-wave scattering:

$$\alpha_0 J_0(kR') + \beta_0 Y_0(kR') = 0 \quad (14)$$

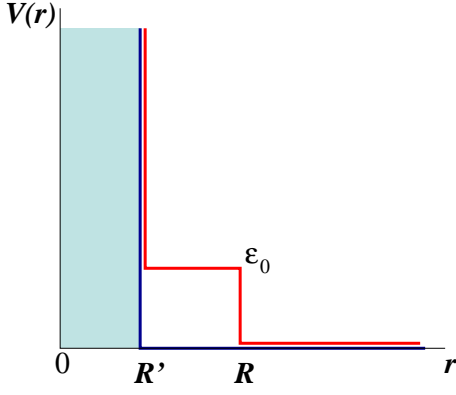


FIG. 2: (Color online). Sketch of the model with circular symmetry used to study the AOC in the presence of localized levels. An infinite potential exists for $0 \leq r \leq R'$, mimicking a vacancy. The perturbation leading to the AOC is modeled as a constant potential, ϵ_0 , for $R' \leq r \leq R$ (see text for details).

The phaseshift induced by the void, before the potential whose effect we want to calculate is turned on, is:

$$\delta_0(k) = \arctan\left(\frac{\beta_0}{\alpha_0}\right) = -\arctan\left(\frac{J_0(kR')}{Y_0(kR')}\right) \xrightarrow{k \rightarrow 0} -\frac{\pi}{2} \frac{1}{\ln(kR')} \quad (15)$$

Next, we model a weak impurity near the void as an isotropic perturbation of depth ϵ_0 , defined in the region $R' \leq |\mathbf{r}| \leq R$. Following eqs. (5,6) and neglecting intervalley scattering, the wavefunction can be written as:

$$\Psi(\mathbf{r}) \equiv \begin{cases} \begin{pmatrix} \alpha' J_0[(k + \epsilon_0)r] + \beta' Y_0[(k + \epsilon_0)r] \\ \alpha' J_1[(k + \epsilon_0)r]e^{i\phi} + \beta' Y_1[(k + \epsilon_0)r]e^{i\phi} \end{pmatrix} & R' \leq r \leq R \\ \begin{pmatrix} \alpha J_0(kr) + \beta Y_0(kr) \\ \alpha J_1(kr)e^{i\phi} + \beta Y_1(kr)e^{i\phi} \end{pmatrix} & R \leq r \end{cases} \quad (16)$$

with boundary conditions:

$$\begin{aligned} \alpha' J_0[(k + \epsilon_0)R'] + \beta' Y_0[(k + \epsilon_0)R'] &= 0 \\ \alpha' J_0[(k + \epsilon_0)R] + \beta' Y_0[(k + \epsilon_0)R] &= \alpha J_0(kR) + \beta Y_0(kR) \\ \alpha' J_1[(k + \epsilon_0)R] + \beta' Y_1[(k + \epsilon_0)R] &= \alpha J_1(kR) + \beta Y_1(kR) \end{aligned} \quad (17)$$

These equations allow us to obtain the phaseshift of the combined system, void and circular impurity, as $\delta = \arctan(\beta/\alpha)$. The overlap between the Slater determinants before and after the impurity potential is switched on, is determined by the phase difference, $\delta - \delta_0$, where δ_0 is given in eq.(15).

Results for the individual phaseshifts δ and δ_0 , as well as their difference are shown in Fig.[3] for $\epsilon_0 = 0.1$, $R' = 0.9$ and $R = 1$. In this regime of energies much lower than ϵ_0 , the phaseshift δ seems to approach δ_0 from below, indicating that the repulsive character of the void is weakened by the additional constant potential. For the small energies close to the Dirac point focused on here, the relative phaseshift, $\delta - \delta_0$, is always finite and seems to approach a constant. This behavior differs strikingly from our findings for clean graphene where the vanishing of the phaseshift at the Dirac point (cf. Fig.[1]) indicates the suppression of AOC. In the presence of voids, the small dependence of the phaseshift induced by an additional external potential on energy near the Dirac point implies that the overlap between Slater determi-

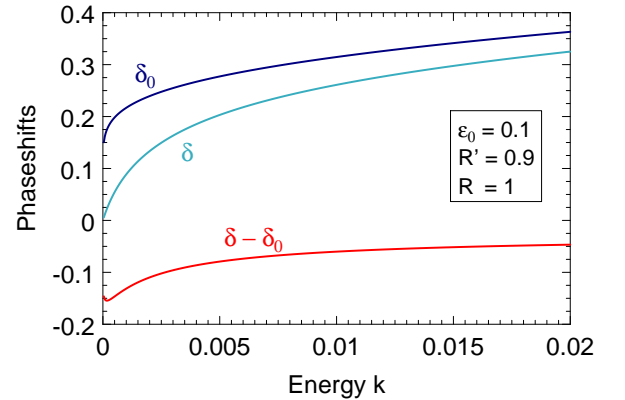


FIG. 3: (Color online). Phaseshift δ_0 induced by a void, the phaseshift δ resulting from the additional switching on of a constant potential, and the resulting relative phaseshift $\delta - \delta_0$ induced by a circular impurity potential surrounding a void (see text for details).

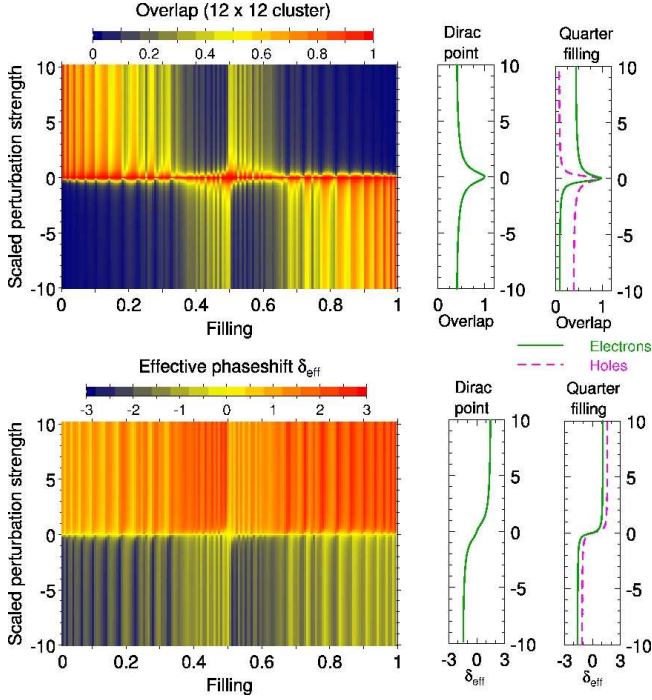


FIG. 4: (Color online). Overlap and effective phaseshift as function of filling and potential strength (see text for details).

nants should scale with the number of electrons in a similar fashion to that in a normal metal with a finite density of states. We shall see in the remainder of this paper that there are indeed considerable differences between clean graphene vs. graphene with localized states, that are visible, e.g., in the behavior of the AOC overlap.

CALCULATION OF THE OVERLAP.

Clean graphene.

The overlap between the unperturbed and perturbed Slater determinants for clean graphene clusters of different sizes has been calculated using the methods described in [21, 22, 23]. The perturbation is a local potential at a given site, $\Delta = \epsilon_0$. Its strength is measured in terms of the scaled perturbation strength $\propto \Delta/d$ with d being the mean level spacing $6/[(N(N+1)-2)]$. Periodic boundary conditions are used in systems with $N \times N$ unit cells, up to $N = 80$; the vertical stripes visible in Fig. [4] are an artefact of the periodic boundary conditions. The results for the overlap for $N = 12$ and different potential strengths (ranging from weak to strong for repulsive as well as attractive perturbations) are shown in Fig. [4]. An effective phaseshift can be defined by dividing the energy shift of the level closest to the Fermi energy by the average level spacing in that energy range. This phaseshift is also shown in Fig. [4].

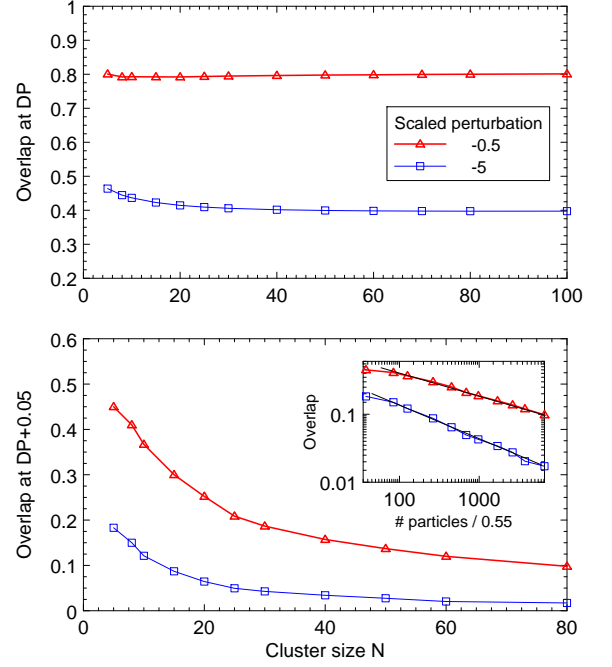


FIG. 5: (Color online). Scaling of the overlap with cluster size N at the Dirac point (DP, $\epsilon_F = 0$, corresponding to a filling of 0.5, top panel) and away from the Dirac point (at fixed filling 0.55, corresponding to $\epsilon_F \sim 0.67$, lower panel). See text for details.

The dependence of the overlap with system size is different at the Dirac point from that at other energies. This dependence is shown in Fig. [5]. The overlap is almost independent of system size at the Dirac point, cf. the upper panel. This result is consistent with the phaseshift analysis, which shows that the phaseshift vanishes at the Dirac point. Indeed, AOC is suppressed at the Dirac point. Away from the Dirac point, the conventional behavior of the AOC overlap is recovered, see the lower panel of Fig. [5]. To this end, AOC overlaps for fillings ranging from 0.54 to 0.56 were averaged over. Clearly, the AOC overlap is no longer suppressed and approaches zero in the thermodynamic limit following the well-known power-law dependence on the number of particles ($\propto [N(N+1)-2]$), cf. inset of Fig. [5].

Graphene with localized states.

The method described in [23] assumes that the wavefunctions of all eigenstates of the unperturbed system have the same weight on the site where the perturbation is turned on. This leads to a considerable simplification of the calculation of the overlap between Slater determinants. Generalization of this method generalized to chaotic mesoscopic systems [21, 22] was done based on

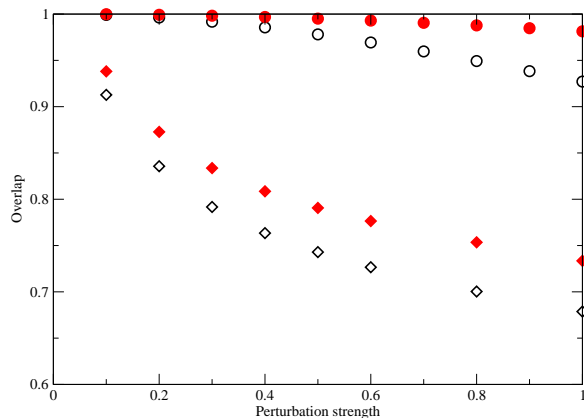


FIG. 6: (Color online). Dependence of the overlap on perturbation strength when the perturbation is turned on near an existing vacancy (empty circles, black), and in clean graphene (filled circles, red). Calculations are done for 12×12 clusters. Circles correspond to one hole in the cluster (Dirac energy, $\epsilon_F = 0$), whereas diamonds characterize a cluster with five holes (corresponding to $\epsilon_F = -0.5$, or a filling of ~ 0.47).

the statistical properties of the chaotic wave functions.

In the presence of a defect which induces a localized state, like a vacancy, the wavefunctions of the unperturbed state, where the localized state is already present, do not possess translational symmetry. Therefore direct diagonalization and calculation of the overlap determinants was used for the study of clusters of moderate sizes.

Results for the overlap for clusters with 12×12 unit cells are shown in Fig.[6]. At the Dirac point, the presence of a vacancy, which induces a localized state, enhances significantly the dependence of the overlap on the strength of the potential. Away from the Dirac point, the difference in the overlap with and without a vacancy is much less pronounced. We show in Fig.[7] the dependence of the overlap with cluster size, at the Dirac energy. As anticipated in the discussion of Fig.[3], the presence of a vacancy near the potential which is turned on modifies significantly the results in comparison with a clean system. In the latter, the dependence on size is negligible, in agreement with the results shown in Fig.[5]. There is, on the other hand, a substantial dependence on cluster size when a vacancy induces a localized state at the Dirac energy.

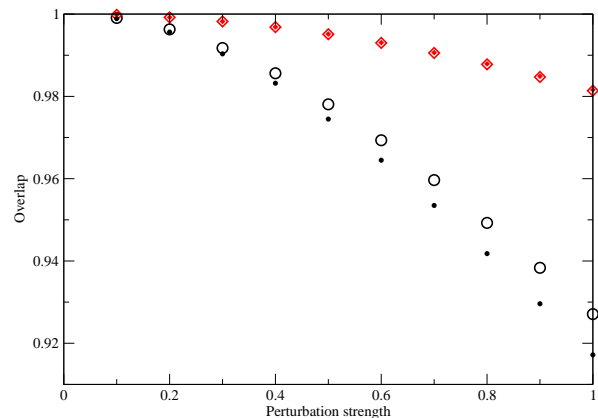


FIG. 7: (Color online). Dependence of the overlap on perturbation strength, at the Dirac energy, when the perturbation is turned on near an existing vacancy (circles, black), and in clean graphene (diamonds, red). Large symbols correspond to a 12×12 cluster and small symbols correspond to a 15×15 cluster.

CONCLUSIONS.

The results presented here show the existence of two regimes for Anderson's orthogonality catastrophe in graphene at low fillings, depending on whether there are localized states at the Dirac energy or not. In the absence of localized states the AOC is suppressed near the Dirac point, in agreement with the vanishing of the density of states at this energy. When localized states are present, the AOC is qualitatively similar to that found in metals with a finite density of states. The latter behavior is a consequence of the fact that, when localized states are sufficiently near the Fermi surface, they contribute to the non adiabatic response of the electron gas. This situation is unique to graphene, as, in most metallic systems, localized states appear at energies well below the Fermi level.

The features discussed above imply that the Kondo effect in graphene also depends on the strength of the scalar potential induced by the magnetic impurity. If the potential induced on the graphene electrons is weak, as when the magnetic impurity is at some distance of the graphene plane, we expect the formation of a Kondo resonance to be suppressed, and the magnetic impurity will give rise to a free magnetic moment. On the other hand, if the magnetic impurity lies within the graphene plane, it will give rise to a strong scalar potential, and possibly to localized states at the Dirac energy. Then, the Kondo effect will not be suppressed, despite the low density of states in graphene near the Dirac energy.

Similar effects can be expected for the Fermi edge singularities induced by electrons tunneling into or out of graphene quantum dots. The strength of the Fermi edge singularities depend on the existence of localized states in the quantum dot. These states will be induced in graphene dots with sharp and rough edges, where, in addition to Coulomb blockade, the AOC associated to electron tunneling will further suppress the conductance at low voltages[13, 14].

ACKNOWLEDGMENTS.

F. G. acknowledges funding from MEC (Spain) through grant FIS2005-05478-C02-01, the European Union Contract 12881 (NEST), and CAM (Madrid) through program CITECNOMIK. M. H. thanks the DFG (Germany) for funding within the Emmy-Noether program.

-
- [1] K. S. Novoselov, A. K. Geim, S. V. Morozov, D. Jiang, Y. Zhang, S. V. Dubonos, I. V. Grigorieva, and A. A. Firsov, *Science* **306**, 666 (2004).
 - [2] C. Berger, Z. M. Song, T. B. Li, X. B. Li, A. Y. Ogbazghi, R. Feng, Z. T. Dai, A. N. Marchenkov, E. H. Conrad, P. N. First, et al., *J. Phys. Chem. B* **108**, 19912 (2004).
 - [3] K. S. Novoselov, A. K. Geim, S. V. Morozov, D. Jiang, M. I. Katsnelson, I. V. Grigorieva, S. V. Dubonos, and A. A. Firsov, *Nature* **438**, 197 (2005).
 - [4] Y. Zhang, Y.-W. Tan, H. L. Stormer, and P. Kim, *Nature* **438**, 201 (2005).
 - [5] A. K. Geim and K. S. Novoselov, *Nature Materials* **6**, 183 (2007).
 - [6] M. Fujita, K. Wakabayashi, K. Nakada, and K. Kusakabe, *J. Phys. Soc. Jpn.* **65**, 1920 (1996).
 - [7] K. Wakabayashi and M. Sigrist, *Phys. Rev. Lett.* **84**, 3390 (2000).
 - [8] M. A. H. Vozmediano, M. P. López-Sancho, T. Stauber, and F. Guinea, *Phys. Rev. B* **72**, 155121 (2005).
 - [9] V. M. Pereira, F. Guinea, J. M. B. Lopes dos Santos, N. M. R. Peres, and A. H. Castro Neto, *Phys. Rev. Lett.* **96**, 036801 (2005).
 - [10] P. W. Anderson, *Phys. Rev. Lett.* **18**, 1049 (1967).
 - [11] P. Nozières and C. T. de Dominicis, *Phys. Rev.* **178**, 1097 (1969).
 - [12] G. D. Mahan, *Many Body Physics* (Plenum Press, New York, 1993).
 - [13] M. Ueda and F. Guinea, *Zeits. für Phys.* **85**, 413 (1991).
 - [14] E. Bascones, C. P. Herrero, F. Guinea, and G. Schön, *Phys. Rev. B* **61**, 16 778 (2000).
 - [15] D. A. Abanin and L. S. Levitov, *Phys. Rev. Lett.* **93**, 126802 (2004).
 - [16] J. S. Bunch, Y. Yaish, M. Brink, K. Bolotin, and P. L. McEuen, *Nano Lett.* **5**, 287 (2005).
 - [17] P. W. Anderson, G. Yuval, and D. R. Hamann, *Phys. Rev. B* **1**, 4464 (1970).
 - [18] P. W. Anderson and G. Yuval, *J. Phys. C* **4**, 607 (1971).
 - [19] F. Guinea, V. Hakim, and A. Muramatsu, *Phys. Rev. B* **32**, 4410 (1985).
 - [20] Y. Gefen, R. Berkowitz, I. V. Lerner, and B. L. Altshuler, *Phys. Rev. B* **65**, 081106 (2002).
 - [21] M. Hentschel, D. Ullmo, and H. U. Baranger, *Phys. Rev. Lett.* **93**, 176807 (2004).
 - [22] M. Hentschel, D. Ullmo, and H. U. Baranger, *Phys. Rev. B* **72**, 035310 (2005).
 - [23] K. Ohtaka and Y. Tanabe, *Rev. Mod. Phys.* **62**, 929 (1990).
 - [24] J. L. Mañes, F. Guinea, and M. A. H. Vozmediano, *Phys. Rev. B* **75**, 155424 (2007).